Acta Biochim Biophys Sin 2026, 58(6): 1342–1355
https://cstr.cn/32197.14.abbs.2025172
https://doi.org/10.3724/abbs.2025172
Original Article

Original Article

Long noncoding RNA LINC02432 inhibits papillary thyroid cancer via promoting ferroptosis

Yilin Zhang[1,†], Chuimian Zeng[1,†], Junxin Chen[1,†], Weijian Ke[1], Yi Zhao[2], Niandong Yi[3], Xueying Chen[4], Jinmei Deng[5], Xianying Zhu[6], Yanbing Li[1,*], and Hongyu Guan[1,*]

[1]Department of Endocrinology and Diabetes Center, The First Affiliated Hospital of Sun Yat-sen University, Guangzhou 510080, China, [2] Department of Immunology, Zhongshan School of Medicine, Sun Yat-Sen University, Guangzhou 510080, China, [3]Department of Microbiology, Zhongshan School of Medicine, Sun Yat-Sen University, Guangzhou 510080, China, [4]Department of Endocrinology, Guangdong Geriatrics Institute, Guangdong Provincial People's Hospital (Guangdong Academy of Medical Sciences), Southern Medical University, Guangzhou 510100, China, [5]Internal Medicine Department, The First Affiliated Hospital of Sun Yat-sen University, Guangzhou 510080, China, and [6] Department of Intensive Care Unit, State Key Laboratory of Oncology in South China, Guangdong Provincial Clinical Research Center for Cancer, Sun Yat-sen University Cancer Center, Guangzhou 510060, China

[†]These authors contributed equally to this work.

*Correspondence address. E-mail: ghongy@mail.sysu.edu.cn (H.G.); liyb@mail.sysu.edu.cn (Y.L.)

Received 13 March 2025 Accepted 27 August 2025 Published 16 December 2025

Abstract

Long noncoding RNAs (lncRNAs) are essential in regulating the development and progression of different types of cancer. However, our insights into their impact and mechanisms in papillary thyroid carcinoma (PTC) are still insufficient. In this study, we investigate the effects of the ferroptosis-associated long noncoding RNA LINC02432 on PTC, which recognizes ferroptosis as a critical mechanism in cancer biology and lncRNAs as significant factors in various malignancies. To identify lncRNAs associated with ferroptosis in PTC, we conduct bioinformatics analyses and perform functional assays to evaluate the biological impact of LINC02432 on PTC cells, as well as its relationship with ferroptosis. Mechanistic studies employ methods such as western blot analysis, flow cytometry, and real-time PCR. Our analysis of transcriptome data from TCGA reveals that LINC02432 is the only lncRNA consistently identified by all 10 machine learning methods used, and its expression is significantly downregulated in PTC. Overexpression of LINC02432 in PTC cells inhibits cell proliferation and migration while promoting ferroptosis through inactivation of the NRF2 pathway. *LINC02432* knockdown in PTC cells yields the opposite result. These findings highlight the potential of LINC02432 as a tumor suppressor in PTC progression, offering new insights into the mechanisms underlying the development and progression of this malignancy.

Key words ferroptosis, LINC02432, NRF2 pathway, papillary thyroid cancer

Introduction

Thyroid cancer (TC) is one of the most prevalent endocrine malignancies globally, with an estimated 586,000 new cases reported in the latest Global Cancer Observatory survey from 2020 [1]. TC can be categorized into several subtypes, namely, papillary thyroid cancer (PTC), follicular thyroid cancer, anaplastic thyroid cancer, and medullary thyroid cancer, with PTC being the dominant subtype, accounting for approximately 80% of cases [2]. While the majority of PTC patients have a favorable prognosis, a subset may experience disease progression, including invasive growth and distant metastasis, leading to poor clinical outcomes [3,4]. Therefore, elucidating the molecular mechanisms underlying PTC progression is crucial for understanding the etiology of this disease.

Ferroptosis, a recently characterized form of programmed cell death, is characterized by the accumulation of iron-dependent lipid peroxides, resulting in phospholipid peroxidation and subsequent cellular damage [5]. Emerging evidence indicates a significant relationship between ferroptosis and TC, with effective induction of ferroptosis shown to markedly inhibit the proliferation of TC cells and impede tumor progression [6]. Additionally, research has demonstrated that hepatic leukemia factor promotes ferroptosis resistance in triple-negative breast cancer cells through gamma-

© The Author(s) 2025. This is an open access article distributed under the terms of the Creative Commons Attribution Non-Commercial License (https://creativecommons.org/licenses/by-nc/4.0/).

glutamyltransferase 1, ultimately facilitating malignant tumor progression [7]. Thus, targeting ferroptosis represents a promising avenue for the development of innovative therapeutic strategies for TC.

Long noncoding RNAs (lncRNAs), which are noncoding RNAs longer than 200 nucleotides, are generated from extensive transcriptional processes [8]. These lncRNAs can interact with diverse cellular biomolecules, including RNA, DNA, and proteins, thereby influencing a range of cellular functions. Dysregulation of lncRNA expression has been implicated in the pathogenesis of various human diseases, including numerous cancer types, highlighting the essential roles of lncRNAs in both cellular health and disease [9]. LncRNAs have been shown to participate in numerous physiological and pathological processes, including inflammation, the immune response, carcinogenesis, and development [10,11]. Aberrant lncRNA expression has been documented in multiple cancers, including PTC [12]. Currently, lncRNAs are recognized for their ability to regulate oncogenes and critical signaling pathways, acting either upstream to initiate these pathways or downstream to modulate their effects [13]. The regulation of tumor suppressors and oncogenes involves various mechanisms, such as the ability of lncRNAs to function as RNA decoys, modulate alternative splicing, and induce epigenetic, transcriptional, and posttranscriptional modifications [14–16]. However, the specific roles of lncRNAs in PTC in the context of ferroptosis remain largely unknown.

In this study, we conducted bioinformatics analyses to identify lncRNAs associated with ferroptosis in PTC. Our functional studies demonstrated that LINC02432 significantly promotes the proliferation, migration, and invasion of PTC cells. Mechanistically, LINC02432 inhibits the activation of the NRF2 pathway, thereby influencing the progression of ferroptosis in PTC. In conclusion, our findings provide new insights into the mechanisms underlying the development and progression of PTC.

Materials and Methods

Exploration of ferroptosis-related lncRNAs

The RNA-seq transcriptome data for thyroid carcinoma (THCA) patients were downloaded from The Cancer Genome Atlas (TCGA). We extracted a total of 415 ferroptosis-related genes (FRGs), which include drivers, suppressors, markers, and unclassified regulators, from the FerrDb database (http://www.zhounan.org/ferrdb/current/) [17]. To identify FRGs and lncRNAs for further investigation, we analyzed the differentially expressed genes (DEGs) and conducted survival analyses. The differentially expressed genes were obtained via the R DESeq2 package, applying screening criteria of $|\log FC| > 1$ and $P < 0.05$. Survival analysis was performed with the survival package, where the criterion for selection was a log-rank test P value of less than 0.05. We subsequently employed Pearson correlation analysis to assess the relationships between lncRNAs and ferroptosis-related genes, establishing a filter standard with a correlation coefficient of 0.5 and a P value threshold of 0.05. We utilized 10 machine learning methods to identify genes associated with the progression-free interval (PFI) in patients with PTC. The methods employed include XGBoost (eXtreme Gradient Boosting), GBM (gradient boosting machine), Bootstrap, robust regression, elastic net, ridge regression, partial least squares (PLS), stability LASSO (least absolute shrinkage and selection operator), supervised principal components (SuperPC), and adaptive LASSO. Each of these techniques was employed to enhance the identification of relevant markers linked to the PFI in PTC patients. All machine learning analyses in our study were performed locally via R version 4.4.2 and its associated packages (*e.g.*, xgboost, glmnet, gbm, superpc, *etc.*). To robustly identify prognostic biomarkers, we independently applied the aforementioned 10 distinct algorithms to rank genes on the basis of their importance scores (*e.g.*, regression coefficients, gain values, and selection frequencies). Each method's raw scores were converted to ranks, and the top 10 genes from each method's list were extracted. The analysis workflow is shown in Supplementary Figure S1.

Cell culture and reagents

The human thyroid epithelial cell line Nthy-ori3-1 and the PTC cell line TPC1 were kindly provided by Prof. Haixia Guan (Guangdong Provincial People's Hospital, Guangzhou, China). The BCPAP and KTC1 cell lines were purchased from the Cell Bank of Type Culture Collection of the Chinese Academy of Sciences (Shanghai, China). Cells were cultured in Dulbecco's modified Eagle's medium (DMEM; Gibco, Carlsbad, USA) supplemented with 10% fetal bovine serum (FBS) (Gibco), 100 U/mL penicillin (Biosharp, Hefei, China), and 100 mg/mL streptomycin (Biosharp) at 37°C in a humidified incubator with 5% CO_2. The apoptosis inhibitor Z-VAD-FMK, the necrosis inhibitor necrostatin-1 (Nec-1), and the ferroptosis inhibitors ferrostatin-1 (Fer-1) and liproxstatin-1 (Lip-1) were purchased from Selleck (Houston, USA).

Patients and tissue specimens

Sixteen pairs of PTC tissues and corresponding adjacent noncancerous thyroid tissues were obtained from the First Affiliated Hospital of Sun Yat-sen University (Guangzhou, China). These samples were frozen in liquid nitrogen until use. Patients were required to have histologically confirmed PTC, complete surgical and follow-up records, and no prior history of thyroid malignancy. We excluded patients with indeterminate pathology, patients receiving neoadjuvant therapies, and those with concurrent malignancies. Informed consent was obtained from all patients, and ethics approval was obtained from the Institutional Research Ethics Committee of the First Affiliated Hospital of Sun Yat-sen University (No. [2021] 087).

Plasmids and construction of stable cell lines

The LINC02432-overexpressing plasmid pCDH-CMV-Homo-LINC02432-EF1-puro and the empty control plasmid pCDH-CMV-MCS-EF1-Puro were generated by and purchased from IGE Biotechnology Co., Ltd. (Guangzhou, China). The plasmid, along with two packaging plasmids, psPAX2 and pMD2.G, was transfected into HEK293T cells via EndoFectin™ Max transfection reagent (GeneCopoeia, Rockville, USA). At 48 h after transfection, the lentivirus-containing supernatant was collected, passed through a 0.22-μm filter, and supplemented with 10 mg/mL polybrene (Biosharp). Stable cell lines were subsequently selected with 2 μg/mL puromycin for two weeks.

Transfection of the lncRNA Smart Silencer

The Smart Silencer targeting LINC02432 was purchased from RiboBio (Guangzhou, China). This Smart Silencer comprises three siRNAs and three antisense oligonucleotides (ASOs). The target sequences of the siRNAs are as follows: 5′-GGTGCTGTCAAGAC TAGAA-3′, 5′-GAAGGTGCTGTCAAGACTA-3′, 5′-GATGAAATCT TATGATATA-3′. The target sequences of the ASOs are as follows:

5′-CACTTATGTACTGCATCAAG-3′, 5′-TTCATGCCAGGA GAAGCCTC-3′, 5′-GAACACTGCCTCATCTATTG-3′. The Smart Silencer negative control (lncRNA Smart Silencer NC #1, lnc3N0000001-1-5; RiboBio) contains no domains homologous to those in humans, mice, or rats. Transfection was performed via EndoFectin™ Max transfection reagent (GeneCopoeia).

RNA extraction and quantitative real-time polymerase chain reaction (qRT-PCR)

The RNA from fresh tissues and cultured cells was extracted with an RNA extraction kit (Tiangen, Beijing, China). cDNA synthesis was performed with 1 μg of total RNA as the template using GoScript Reverse Transcription Mix (Promega, Madison, USA). The GoTaq qPCR Master Mix (Promega) was used to quantify the mRNA levels of the indicated genes in triplicate on a QuantStudio 5 Real-Time PCR System (Applied Biosystems, Foster City, USA). *GAPDH* was used as an internal control to normalize the indicated genes, and all reactions were performed in triplicate. The relative expression levels were calculated via the $2^{-\Delta\Delta ct}$ method. The primer sequences are listed in Supplementary Table S1.

Western blot analysis

The cells were rinsed two times with precooled PBS buffer and lysed in RIPA buffer (Beyotime, Shanghai, China) supplemented with protease and phosphatase inhibitor cocktail (Epizyme, Shanghai, China). The cell lysates were incubated for 5 min on ice and clarified via centrifugation at 12,000 *g* for 10 min. Then, a bicinchoninic acid assay kit (BCA; Biosharp) was used to determine the protein concentrations. Total protein samples were mixed (4:1) with 5× SDS-PAGE loading buffer (Epizyme) and denatured at 100°C for 5 min. The protein samples (20–30 μg) were resolved via 10% SDS-PAGE, transferred to polyvinylidene fluoride (PVDF) membranes (Millipore, Burlington, USA), blocked with 5% skim milk for 1 h at room temperature, and then incubated with primary antibodies overnight at 4°C. After three TBST washes, secondary antibodies labeled with horseradish peroxidase (CST, Danvers, USA) were applied at room temperature for 1 h. The immunoblotting signals were visualized via an enhanced chemiluminescence (ECL) detection kit (Millipore), and the signal was detected via the ECL western blotting substrate (Tanon, Shanghai, China). A nuclear protein extraction assay was performed via a Nuclear and Cytoplasmic Protein Extraction Kit (Beyotime). ImageJ was used for quantitative grayscale analysis. The primary antibodies used are listed in Supplementary Table S2.

CCK-8 assay

For the cell viability assay, indicated cells were trypsinized and seeded into 96-well plates at a density of 2×10^3 cells per well in equal volumes of medium. On day 1, 2, 3, 4, and 5, the culture medium was carefully removed from each well, and 100 μL of fresh culture medium containing 10 μL CCK-8 solution (Beyotime) was added to each well. The plates were then incubated at 37°C for 1 h. Absorbance was measured at 450 nm using a microplate reader (BioTek, Winooski, USA) to quantify cell viability.

Colony formation assay

Cells were trypsinized into single-cell suspensions and counted. A total of 1×10^3 cells were seeded per well of a 6-well plate. After macroscopic colonies became visible, the cells were washed three times with PBS, fixed with 4% paraformaldehyde for 10 min, and stained with 0.1% crystal violet solution. The plates were then photographed and the colonies were quantified via ImageJ.

Wound healing assay

The cell migration ability was examined via a wound-healing assay. Briefly, cells were seeded in 6-well plates and cultured to a confluent monolayer at 90%–95% confluence. Then, the wounds were created by scratching the cell monolayer with a micropipette tip at 0 h. The cells were washed with PBS to remove nonadherent cells, and wound closure was photographed under a CKX53 microscope (Olympus, Tokyo, Japan) after they were allowed to migrate for 24 h in serum-free medium. The distances between the wound edges were determined via Image-Pro Plus software (Media Cybernetics, Rockville, USA).

Transwell assay

Briefly, the indicated cells (1.5×10^5 for TPC1, 1.0×10^5 for BCPAP, and 1.5×10^5 for KTC1) suspended in 200 μL of serum-free medium were added to the apical chambers of Transwell chambers (Corning, Corning, USA) precoated with or without Matrigel (R&D, Minneapolis, USA). Moreover, the bottom chamber was filled with 650 μL of medium containing 10% FBS. After incubation for 24 h (migration assay) or 48 h (invasion assay), the noninvading or nonmigrating cells on the upper side of the inserts were removed by wiping with cotton swabs. The cells that subsequently migrated to the lower surface of the chamber membrane were fixed with 4% paraformaldehyde, stained with 0.1% crystal violet for 30 min, and counted under the CKX53 microscope (Olympus). Each experiment was performed in triplicate and repeated three times.

EdU incorporation assay

The EdU incorporation assay was carried out as previously described [17], using the BeyoClick™ EdU Cell Proliferation Kit (Beyotime) according to the manufacturer's protocol. Briefly, indicated cells were seeded in triplicate into 48-well plates and cultured for 24 h. The cells were then pulsed with 10 μM EdU for 1 h at 37°C. Following incubation, cells were fixed with 4% paraformaldehyde for 30 min and permeabilized with 0.5% Triton X-100 for 20 min at room temperature. Click-iT reaction was performed by incubating the cells with 1× EdU Click-iT reaction cocktail for 30 min. Subsequently, the cell nuclei were stained with DAPI for 10 min. EdU-positive cells were visualized under the CKX53 microscope (Olympus). Each experiment was repeated three times.

Flow cytometry analysis

The indicated cells were harvested and washed three times with ice-cold PBS for cell cycle analysis. The cells were subsequently fixed with 70% ethanol at 4°C overnight. Afterward, the cells were washed with ice-cold PBS and dyed with PI/RNase staining buffer (Beyotime) for 30 min at 37°C. The cells were analyzed on a cytoFLEX flow cytometer (Beckman-Coulter, Brea, USA).

Measurement of intracellular reactive oxygen species (ROS) production

BCPAP and TPC1 cells were harvested, washed once with DMEM, and incubated with 10 μM DCFH-DA (Beyotime) at 37°C under 5% CO_2 for 15 min in the dark. The cells were then washed twice and resuspended in PBS for detection with a cytoFLEX flow cytometer

(Beckman-Coulter).

Measurement of the mitochondrial membrane potential

The mitochondrial membrane potential (MMP) was assessed via the fluorescent indicator JC-1 (Beyotime). The indicated cells were incubated with 200 μM JC-1 for 20 min at 37°C. JC-1 penetrates the mitochondrial matrix, forming polymers that emit red fluorescence. Conversely, at a low MMP, JC-1 remains as a monomer in the cytoplasm, producing green fluorescence. The following two washes with PBS were used to eliminate residual reagents, and images were captured via a CKX53 microscope (Olympus).

Iron/MDA/GSH assays

An iron assay kit (Abcam, Cambridge, UK) was used to determine the intracellular ferrous iron levels according to the manufacturer's protocol. MDA levels were determined via a lipid peroxidation (MDA) assay kit (Sigma-Aldrich, St Louis, USA) according to the manufacturer's protocol. GSH levels were determined via a GSH-Glo™ glutathione assay kit (Promega) according to the manufacturer's protocol.

Mouse experiments

All animal experiments were conducted following national and international guidelines and approved by the Animal Care Committee of Sun Yat-sen University (No. 2023–2729). Six-week-old female BALB/c nude mice (GemPharmatech Co., Ltd, Foshan, China) were housed under specific pathogen-free conditions on a 12-h light/dark cycle with free access to food and water. For the tumorigenicity assay, stably transfected BCPAP cells (5×10^6 cells per mouse) were subcutaneously injected into nude mice. Each group consisted of five mice. Tumor size was measured every five days via a caliper. The volume was calculated via the following formula: $V = (L \times W^2)/2$, where L represents the largest diameter (in millimeters) and W represents the shortest diameter (in millimeters). The tumor weights were recorded, and the animals were euthanized after five weeks. The tumor tissues were subjected to immunohistochemistry.

Immunohistochemistry

Paraffin-embedded sections were incubated in an incubator at 65°C for 1 h, deparaffinized in xylene, rehydrated through graded ethanol, and subjected to heat-induced antigen retrieval in 10 mM citrate buffer (pH 6.0) for 3 min at 95°C. After being blocked with 5% BSA for 30 min, the sections were incubated with primary antibody diluted in PBS containing 5% BSA at 4°C overnight, followed by incubation with HRP-conjugated secondary antibody for 1 h at room temperature. Antibody binding was visualized using DAB substrate (5 min), and tissues were counterstained with Mayer's hematoxylin, dehydrated, and mounted. Images were captured using a BX53 microscope (Olympus).

Statistical analysis

Statistical analysis was performed with GraphPad Prism 9 (GraphPad Software, Inc., La Jolla, USA), SPSS 23 (IBM, Armonk, USA), or R version 4.2.0 (R Foundation for Statistical Computing, Vienna, Austria). The data are presented as the mean ± standard deviation (SD) from at least three independent experiments unless otherwise indicated. Student's *t*-test or Wilcoxon test was used for two-group comparisons. To compare the significance of survival analysis differences, log-rank test was employed. Associations between LINC02432 expression and clinical characteristics were examined via χ^2 tests. The relationships between LINC02432 and the disease-free interval (DFI) or PFI were assessed through Cox proportional hazards regression. The Pearson correlation test was used for correlation analyses. $P < 0.05$ was considered to indicate statistical significance.

Results

LINC02432 is identified as a ferroptosis-related lncRNA

In our comprehensive analysis, we initially identified 67 differentially expressed FRGs (Supplementary Table S3) and 1770 differentially expressed lncRNAs (Supplementary Table S4) through differential expression analyses. Following survival analyses, 14 FRGs and 217 lncRNAs were obtained. Subsequently, coexpression analysis between these lncRNAs and FRGs revealed 66 candidate lncRNAs (Supplementary Table S5). To further refine our focus, we employed 10 distinct machine learning approaches to explore genes associated with the PFI in patients with PTC (Supplementary Figure S1). The top 10 genes identified by each method were compiled. Figure 1A illustrates the frequency with which these top genes were consistently identified across the various methods. Notably, LINC02432 emerged as the sole molecule detected across all 10

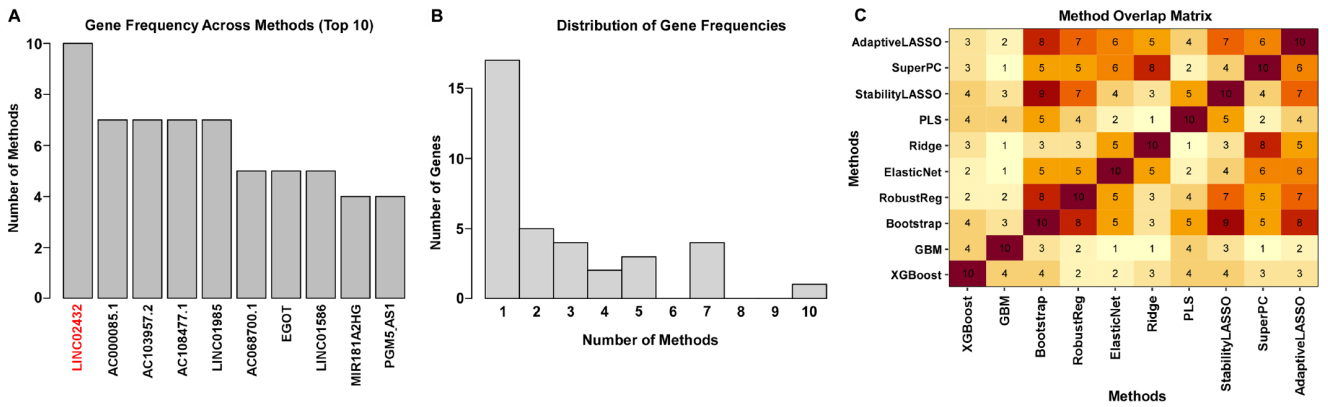


Figure 1. LINC02432 is identified as a ferroptosis-related lncRNA (A) Gene frequency bar plot. The frequency of each gene across all methods was calculated. (B) Frequency distribution histogram. This histogram depicts the distribution of gene frequencies across all methods. (C) Method overlap heatmap. A matrix is created to show the number of overlapping genes between each pair of methods.

methods, underscoring its potential critical role. Figure 1B provides a histogram of the gene frequency distribution, offering a visual representation of gene selection consistency. Additionally, Figure 1C presents an overlap matrix detailing the number of genes shared between each pair of methods. On the basis of these findings, our study focused on elucidating the clinical and biological significance of LINC02432 in the context of PTC.

LINC02432 is downregulated in PTC tissues and is significantly associated with clinical outcomes

We subsequently analyzed the expression of LINC02432 in PTC tissues and normal thyroid tissues via the TCGA database. The results revealed that LINC02432 was downregulated in PTC tissues (Figure 2A,B). We subsequently collected 16 pairs of PTCs and their corresponding adjacent noncancerous thyroid tissues to verify the expression of LINC02432 in PTCs. The qRT-PCR results were consistent with the analysis of the TCGA datasets (Figure 2C). We also detected the expression of LINC02432 in PTC cell lines (IHH4, KTC1, TPC1, and BCPAP) and in the normal thyroid cell line Nthy-ori3-1. Compared with that in Nthy-ori3-1 cells, the expression of LINC02432 in PTC cells was significantly lower (Supplementary Figure S2). Next, Kaplan-Meier survival analyses were performed to examine the associations between LINC02432 and clinical outcomes in PTC patients via the TCGA-THCA dataset. As shown in Figure 2D,E, LINC02432 downregulation was significantly associated with a shorter PFI (P = 0.0013) and DFI (P = 0.0012) in PTC. Subsequent univariate and multivariate Cox regression analyses indicated that low expression of LINC02432 independently increased the risk for both PFI and DFI (Figure 2F,G).

LINC02432 is associated with clinicopathologic features and dedifferentiation indicators

On the basis of the quartiles of LINC02432 expression, we divided the samples in the TCGA-THCA dataset into four groups and selected the top 25% and bottom 25% for gene set enrichment analyses (Figure 3A). The LINC02432-low group was significantly enriched in the gene signatures "DELYS_THROID_CANCER_UP" and "FONTAINE_PAPILLARY_THYROID_CARCINOMA_UP" (Figure 3B, the gene sets were obtained from the C2 curated gene sets of the Molecular Signatures Database, https://www.gsea-msigdb.org/gsea/msigdb/human/genesets.jsp), suggesting a potential role of LINC02432 in negatively regulating PTC pathogenesis. We further analyzed the associations of LINC02432 with clinicopathologic features and thyroid differentiation. As shown in Table 1 and Figure 3C, LINC02432 expression is not significantly correlated with age or sex. However, it is significantly negatively associated with T classification, lymph node metastasis, TNM stage, extrathyroidal extension, and BRAF mutation. Thyroid differentiation is critical in TC [18]. Aberrant dedifferentiation is a pivotal factor in the genesis of tumors, and the degree of differentiation of TCs is closely correlated with their degree of malignancy. Moreover, inhibition of dedifferentiation can significantly suppress the progression of TC [19]. Furthermore, by analyzing the correlation between LINC02432 expression and the expression levels of 16 thyroid differentiation-associated genes (PAX8, TG, TPO, THSR, NKX2-1, SLC5A5, SLC5A8, SLC26A4, GLIS3, FOXE1, THRA, THRB, DUOX1, DUOX2, DIO1, and DIO2) via data from the TCGA-THCA dataset, we found that the expression of LINC02432 is positively correlated with the expression of genes associated with thyroid differentiation (Figure 3D). The thyroid differentiation score (TDS) is an algorithm used to evaluate the degree of TC differentiation [20]. We found that samples exhibiting higher LINC02432 expression presented increased TDS. In contrast, samples with lower LINC02432 expression presented a reduced degree of differentiation (Figure 3E). Overall, we deduce that low LINC02432 expression in PTC correlates with clinicopathologic features and dedifferentiation indicators.

Table 1. Correlations between LINC02432 expression and clinicopathologic variables in patients with PTC in the TCGA-THCA dataset

Clinicopathologic variables (n)	LINC02432 expression		P value
	Low	High	
Age (years)			
<45 (223)	116	107	0.440
≥45 (272)	132	140	
Gender			
Male (130)	72	58	0.161
Female (365)	176	189	
T classification			
T1+T2 (307)	129	178	**<0.001**
T3+T4 (186)	117	69	
Unknown (2)			
Lymph node metastasis			
Absent (226)	94	132	**0.001**
Present (219)	128	91	
Unknown (50)			
TNM stage			
I+II (328)	148	180	**0.003**
III+IV (165)	98	67	
Unknown (2)			
Extrathyroidal extension			
Absent (328)	142	186	**<0.001**
Present (149)	96	53	
Unknown (18)			
BRAF status			
Wildtype (213)	66	147	**<0.001**
Mutation (282)	181	101	

LINC02432 does not have protein-coding potential

Our analysis with the Coding-Potential Assessment Tool (CPAT) [21] and the Coding Potential Calculator (CPC) [22] indicated that the LINC02432 transcript has no protein-coding potential (Figure 4A), and the ORF Finder at the National Center for Biotechnology Information (NCBI) revealed that LINC02432 does not contain any long open reading frames (ORFs) exceeding 100 amino acids (Figure 4B). Moreover, accumulating evidence has shown that the biological functions of lncRNAs are closely associated with their subcellular localization [23]. We examined the subcellular localization of LINC02432 by cellular fractionation and qRT-PCR assays, and found that it resides in the nuclear and cytoplasmic fractions (Figure 4C). The predicted secondary structure of the full-length LINC02432 was analyzed by AnnoLnc2 (https://annolnc.

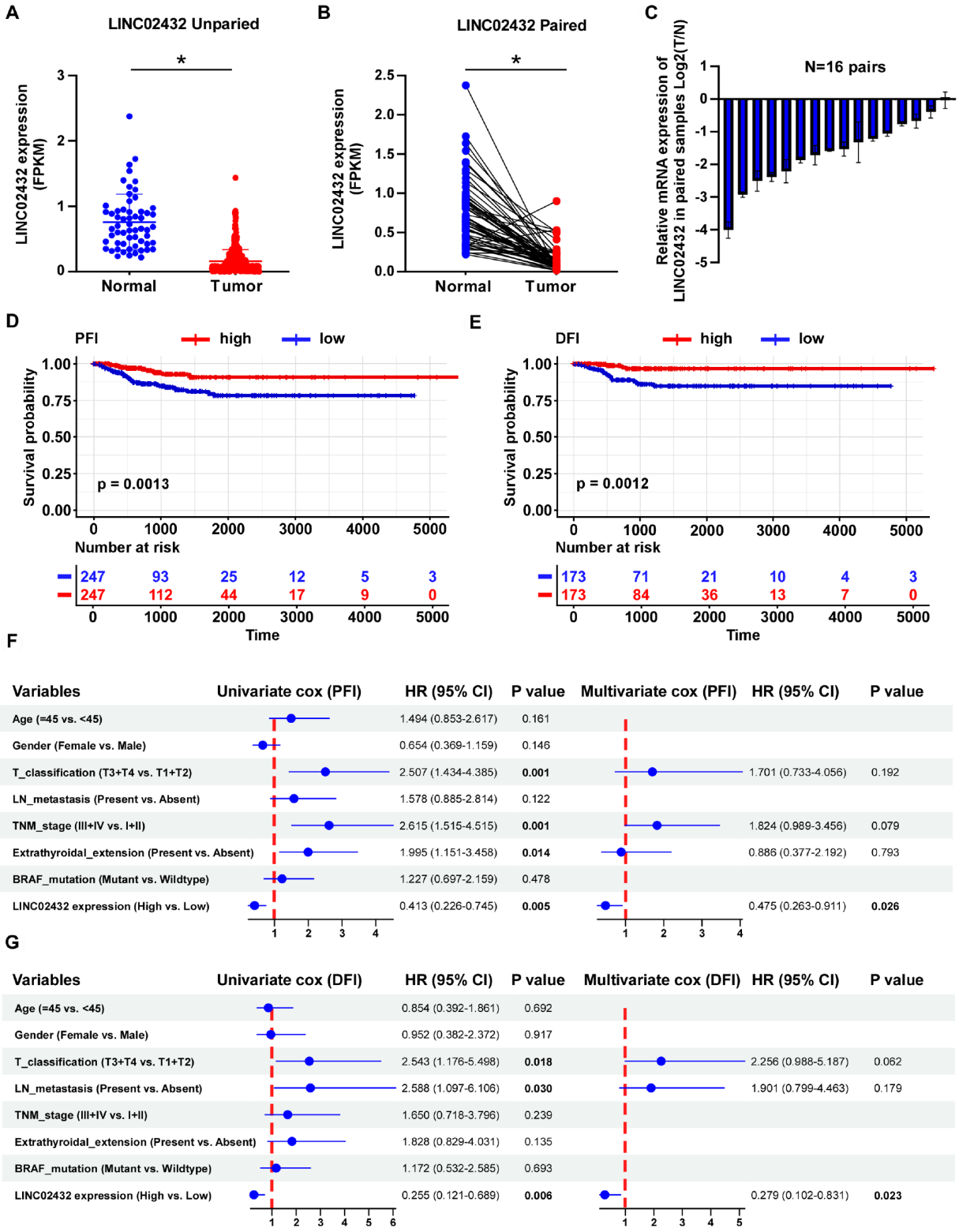


Figure 2. The downregulation of LINC02432 in PTC tissues is significantly correlated with clinical outcomes (A,B) Expression levels of LINC02432 in PTC tissues versus normal thyroid tissues were analyzed via data from the TCGA database. (C) qRT-PCR was performed to assess LINC02432 expression in 16 paired samples of PTCs and their corresponding adjacent noncancerous thyroid tissues. (D,E) Kaplan-Meier survival analyses were conducted to evaluate the relationship between LINC02432 expression and clinical outcomes in PTC patients utilizing the TCGA dataset. (F,G) Univariate and multivariate Cox regression analyses were performed to assess the DFI and PFI associated with LINC02432 expression. Statistical significance was defined as $P \geq 0.05$ (not significant, NS); $^*P < 0.05$ indicates statistical significance.

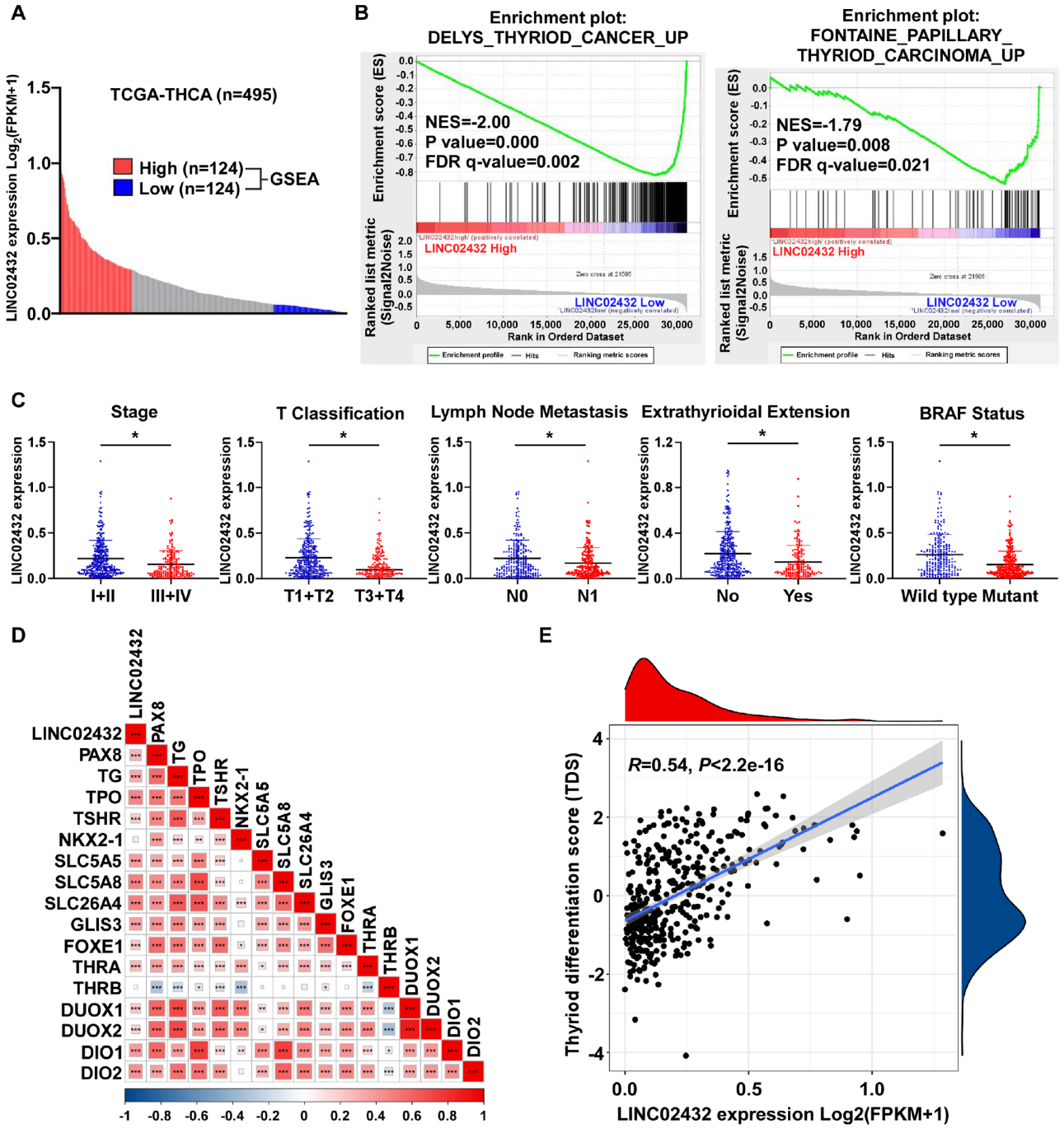


Figure 3. Correlation of LINC02432 expression with clinicopathologic features and dedifferentiation in PTC (A) Based on the quartiles of LINC02432 expression, samples in the TCGA-THCA dataset were divided into four groups. The top 25% and bottom 25% of samples were selected for subsequent GSEA. (B) GSEA was performed to compare the LINC02432-high group with the LINC02432-low group. (C) The relationships between LINC02432 expression and clinicopathologic features, including T classification, lymph node metastasis, TNM stage, extrathyroidal extension, and BRAF mutation status, were assessed. (D) The associations between LINC02432 expression and the expression levels of 16 thyroid differentiation-associated genes (*PAX8*, *TG*, *TPO*, *THSR*, *NKX2-1*, *SLC5A5*, *SLC5A8*, *SLC26A4*, *GLIS3*, *FOXE1*, *THRA*, *THRB*, *DUOX1*, *DUOX2*, *DIO1*, and *DIO2*) were analyzed. (E) The correlation between LINC02432 expression and the thyroid differentiation score (TDS) was evaluated. A *P* value of ≥ 0.05 was considered not significant (NS); **P* < 0.05 indicates statistical significance.

gao-lab.org/), as shown in Figure 4D. In summary, our data demonstrate that LINC02432 is downregulated in PTC, resides in both nuclear and cytoplasmic fractions, and lacks protein-coding potential.

LINC02432 suppresses the proliferation, invasion, and migration of PTC cells

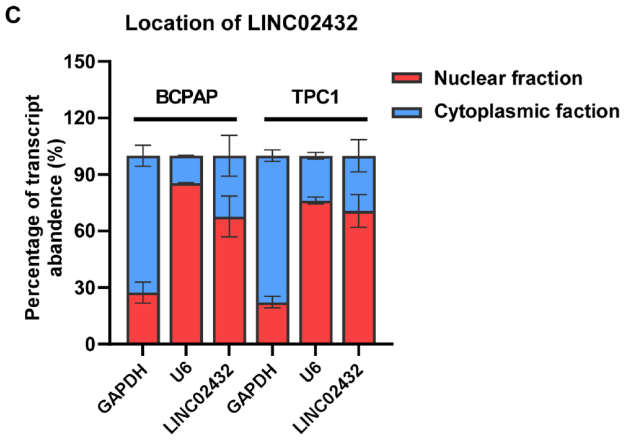
To delineate the role of LINC02432 in PTC, we established stable overexpression of LINC02432 in the PTC cell lines BCPAP and

A

Method	Coding Probability	Coding Label
CPAT	0.035184695309125	noncoding
CPC	0.0240875	noncoding

B

Label	Strand	Frame	Start	Stop	Length (nt|aa)
ORF4	-	1	794	555	240|79
ORF2	+	1	652	807	156|51
ORF6	-	3	828	700	129|42
ORF5	-	2	289	188	102|33
ORF1	+	1	466	543	78|25
ORF3	+	2	530	607	78|25



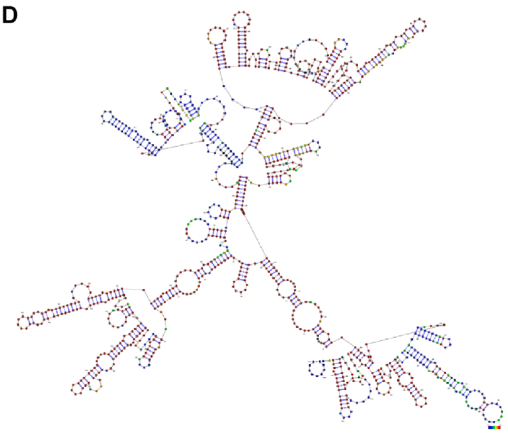


Figure 4. Protein-coding potential and structural analysis of LINC02432 (A) The protein-coding potential of LINC02432 was evaluated via CPAT and CPC analysis tools. (B) Analysis of LINC02432 sequences via ORF Finder. (C) qRT-PCR was conducted to assess the expression levels of *GAPDH* (cytoplasmic control), *U6* (nuclear control), and LINC02432 in the nuclear and cytoplasmic fractions. (D) The secondary RNA structure of LINC02432 was predicted via AnnoLnc2.

TPC1, which have relatively low expression levels of LINC02432 (Figure 5A and Supplementary Figure S2). The CCK-8 assay revealed that LINC02432 overexpression significantly suppressed the growth of these cells compared with their vector-control counterparts (Figure 5B). Additionally, the results of the EdU staining assays revealed a marked reduction in the percentage of positively stained cells, indicating decreased proliferation (Figure 5C). Flow cytometry analysis further revealed that LINC02432 overexpression resulted in cell cycle arrest, with an increased proportion of cells in the G0/G1 phase (Figure 5D). Moreover, the colony formation assay indicated a significant reduction in colony number, reflecting diminished proliferative capacity in cells overexpressing LINC02432 (Figure 5E,F). Wound healing, Transwell migration and invasion assays revealed a substantial decrease in the migratory and invasive ability of BCPAP and TPC1 cells upon LINC02432 overexpression compared with that of vector controls (Supplementary Figure S3A–D). We next performed *LINC02432* knockdown via Smart Silencer in the KTC1 cell line, which has a relatively high expression level of LINC02432. (Supplementary Figures S2 and S4A). As shown in Supplementary Figure S4B–F, knockdown of *LINC02432* significantly promoted KTC1 cell proliferation, invasion, and migration. Together, these findings indicate that LINC02432 plays important roles in the proliferation, invasion, and migration of PTC cells.

LINC02432 suppresses tumor growth *in vivo*

To investigate the role of LINC02432 in the progression of PTC *in vivo*, we subcutaneously injected the indicated cell lines into nude mice. The results demonstrated that the overexpression of LINC02432 significantly inhibited xenograft tumor growth. As shown in Figure 6A, photographs of the excised tumors revealed that the tumors in the LINC02432-overexpressing groups were significantly smaller than those in the control group. qRT-PCR was then performed to validate LINC02432 overexpression in xenograft tissues (Figure 6B). Furthermore, the tumor growth curves presented in Figure 6C indicated a marked reduction in tumor volume over time in the LINC02432-overexpressing mice compared with the control mice. As shown in Figure 6D, tumors from LINC02432-overexpressing mice weighed significantly less than those from control mice. Moreover, IHC analysis of Ki67 confirmed a significant decrease in the percentage of Ki67-positive cells, indicating reduced cellular proliferation within the tumors (Figure 6E,F). Collectively, these results provide strong evidence that LINC02432 suppresses tumor growth *in vivo*.

Overexpression of LINC02432 leads to ferroptosis in PTCs

To further elucidate the relationship between LINC02432 and ferroptosis in PTC cells, we treated BCPAP and TPC1 cells overexpressing LINC02432 with the apoptosis inhibitor Z-VAD-FMK, the necrosis inhibitor Nec-1, and the ferroptosis inhibitors Fer-1 and Lip-1. This was done to determine whether ferroptosis was the primary mechanism by which LINC02432 induces cell death. The results from the CCK-8 assay indicated that, compared with the other inhibitors, the addition of Fer-1 or Lip-1 to PTC cells overexpressing LINC02432 significantly reversed cell death (Figure 7A), suggesting that LINC02432 predominantly promotes cell death through the regulation of ferroptosis. Additionally, qRT-PCR analysis showed that the expression of prostaglandin-endoperoxide synthase 2 (PTGS2), a marker of ferroptosis which is upregulated in response to the lipid peroxides generated during the process, was significantly elevated (Figure 7B). Moreover, the levels of the ferroptosis markers MDA and Fe^{2+} were elevated in BCPAP and

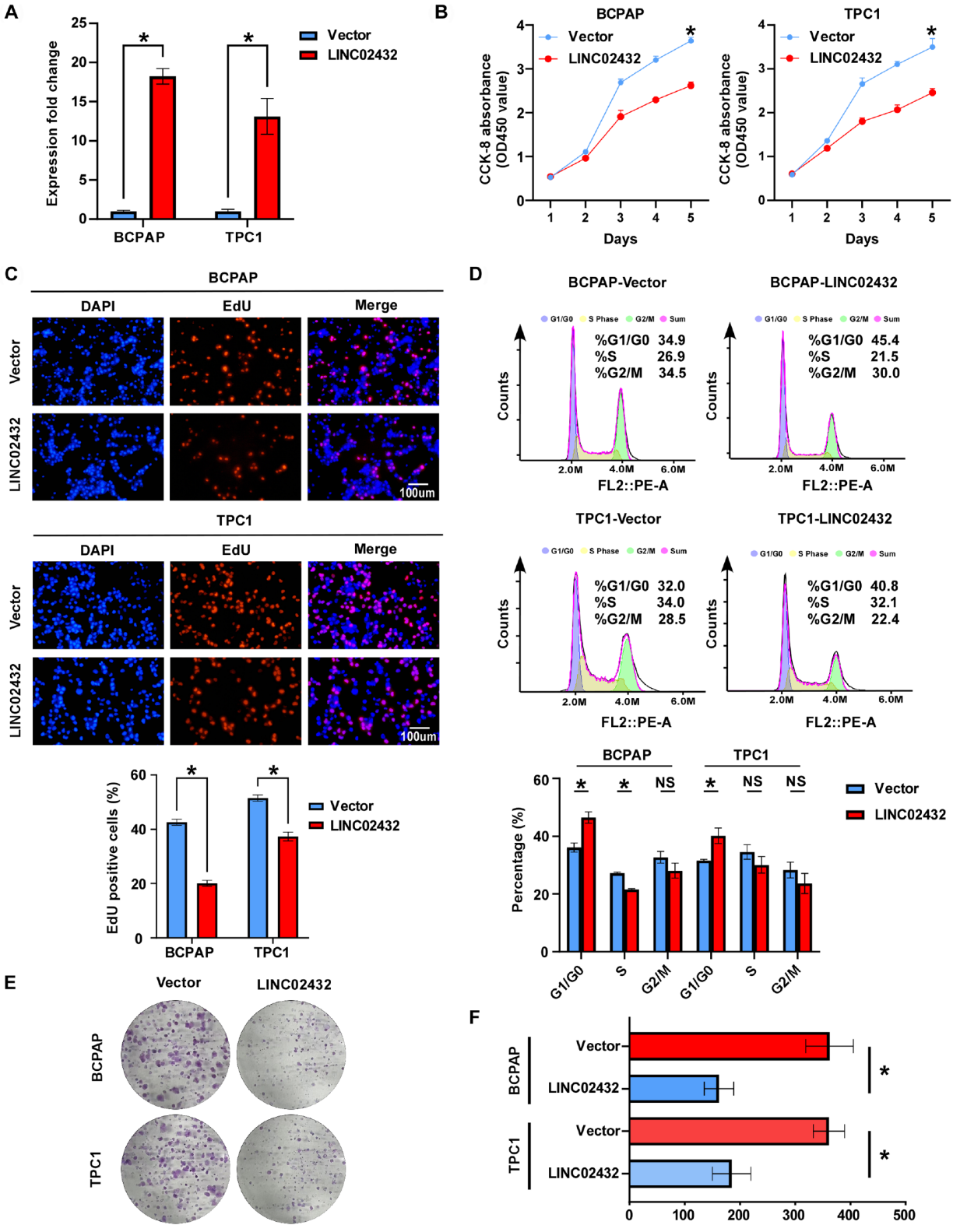


Figure 5. Overexpression of LINC02432 inhibits the proliferative ability of PTC cells (A) qRT-PCR was utilized to confirm the overexpression of LINC02432 in BCPAP and TPC1 cells. (B) CCK-8 assays were performed to investigate the effect of LINC02432 on the viability of the indicated PTC cells at specified time points. (C) Representative images and relative quantification of EdU incorporation assays. (D) Representative images and quantification of the proportions of PTC cells in the G0/G1, S, and G2/M phases, as determined by flow cytometry analysis. (E,F) Representative images and relative quantification of colony formation assays for the indicated cells. The data are presented as the mean ± SD from three independent experiments. A P value of ≥ 0.05 was considered not significant (NS); *P < 0.05 indicates statistical significance.

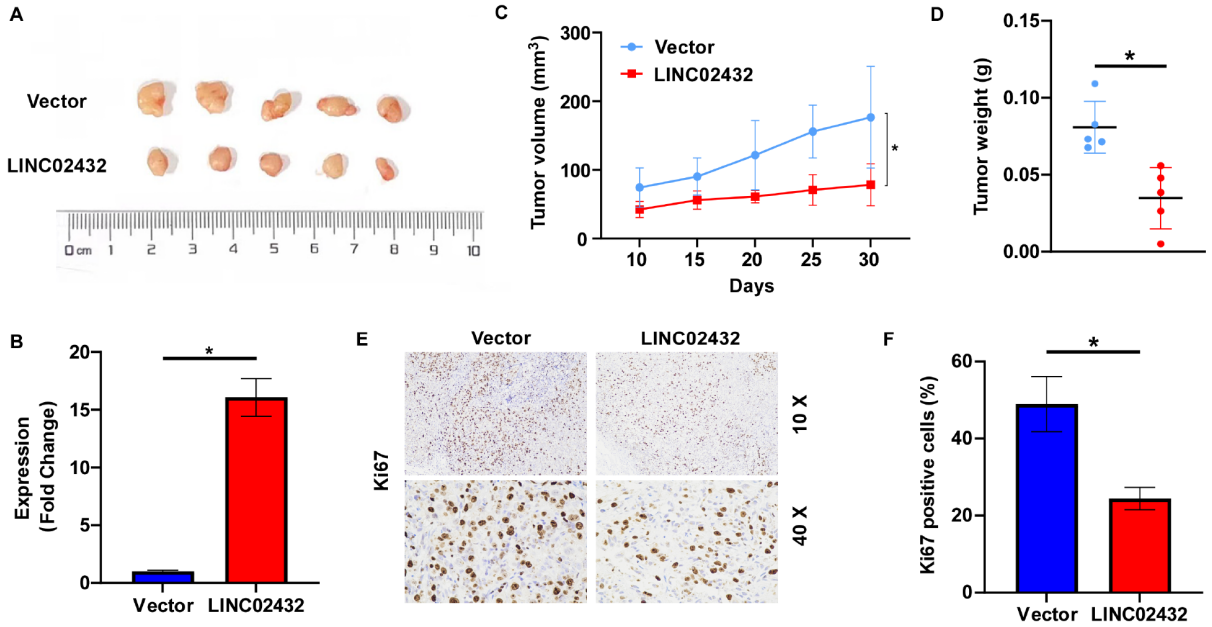


Figure 6. LINC02432 suppresses the tumorigenesis of thyroid cancer cells *in vivo* (A) Images of subcutaneous BCPAP xenografts from the vector control and LINC02432-overexpressing groups ($n = 5$ mice per group). (B) qRT-PCR was utilized to confirm the overexpression of LINC02432 in the subcutaneous BCPAP xenografts. (C) Growth curves of BCPAP xenografts were generated via a digital caliper. (D) Weights of BCPAP xenografts at the end of the experiment. (E) Representative images of Ki67 IHC staining in BCPAP xenografts from the vector control and LINC02432-overexpressing groups. (F) Quantitative analysis showing the percentage of Ki67-positive cells in BCPAP xenografts from the vector control and LINC02432-overexpressing groups. The data are presented as the mean ± SD from three independent experiments. $^*P < 0.05$ indicates statistical significance.

TPC1 cells overexpressing LINC02432 (Figure 7C,D), whereas the GSH level was decreased (Figure 7E), and ROS expression was significantly increased (Figure 7F). Another ferroptosis marker, 4-HNE, was also found to be increased in LINC02432-overexpressing tumors compared with controls (Figure 7G), as revealed by western blot analysis. In addition, compared with empty vector control cells, cells overexpressing LINC02432 presented a reduction in the MMP, preventing JC-1 monomers from entering the mitochondrial matrix to form JC-1 polymers, which indicates a decline in the mitochondrial functional status (Figure 7H). Moreover, *LINC02432* knockdown in KTC1 cells reduced the levels of proferroptotic markers (MDA and Fe^{2+}) but significantly increased the content of GSH, a key ferroptosis suppressor (Supplementary Figure S5A–C). In summary, these findings suggest the critical role of LINC02432 in the regulation of ferroptosis activity.

LINC02432 inhibits the NRF2 pathway via upregulation of KEAP1 in PTC cells

To elucidate the molecular mechanisms by which LINC02432 promotes ferroptosis in PTC development, we conducted qRT-PCR and western blot analyses to evaluate its effects on several ferroptosis-related molecules [24]. We assessed the expression levels of various proteins associated with the ferroptosis pathway and found that NRF2 protein level was decreased in response to LINC02432 overexpression. This reduction was correlated with changes in the expression levels of its downstream targets, SLC7A11 and GPX4 [25] (Figure 8A). Additionally, we observed that the expression of KEAP1, a well-known negative regulator of NRF2, was upregulated following LINC02432 overexpression in BCPAP and TPC1 cells, but downregulated following *LINC02432* knockdown in KTC1 cells [26] (Figure 8A and Supplementary Figure S7A). Because NRF2 translocates to the nucleus to bind to the antioxidant response element (ARE) [26] and leads to the activation of downstream genes, we investigated the nuclear translocation of NRF2. As shown in Figure 8B and Supplementary Figure S7B, LINC02432 overexpression resulted in reduced nuclear translocation of NRF2. The mRNA expression levels of NRF2 downstream genes, including *SLC7A11*, *GPX4*, *GCLC*, *HMOX1*, and *NQO1*, were decreased in PTC cells with LINC02432 overexpression (Figure 8C). The protein levels of GCLC, HO-1, and NQO1, which are encoded by *GCLC*, *HMOX1*, and *NQO1* respectively, were also decreased. (Figure 8D and Supplementary Figure S7C). The activity of NRF2 is regulated primarily through a dynamic process involving continuous protein synthesis and degradation. KEAP1 functions as a substrate adapter for the Cullin 3 (CUL3)-based E3-ligase complex, targeting NRF2 for ubiquitination and subsequent degradation via the 26S proteasome [27]. Moreover, we found that the *NRF2* mRNA level remained unchanged (Figure 8E). Therefore, we evaluated NRF2 ubiquitination levels and degradation rates. Our findings indicated that LINC02432 overexpression accelerated NRF2 degradation in both BCPAP and TPC1 cells (Figure 8F) and increased NRF2 ubiquitination, as detected by immunoprecipitation analysis and western blot analysis (Figure 8G). We next examined the NRF2 pathway in *LINC02432*-knockdown KTC1 cells. As shown in Supplementary Figures S6A and S7D, *LINC02432* knockdown reduced KEAP1 protein level while upregulating NRF2 protein and its downstream targets (SLC7A11, GPX4, HO-1, NQO1). Enhanced nuclear translocation of NRF2 was concurrently observed in *LINC02432*-knockdown KTC1 cells (Supplementary Figures S6B and S7E). In conclusion, overexpression of LINC02432 enhances the ubiquitination and proteasomal degrada-

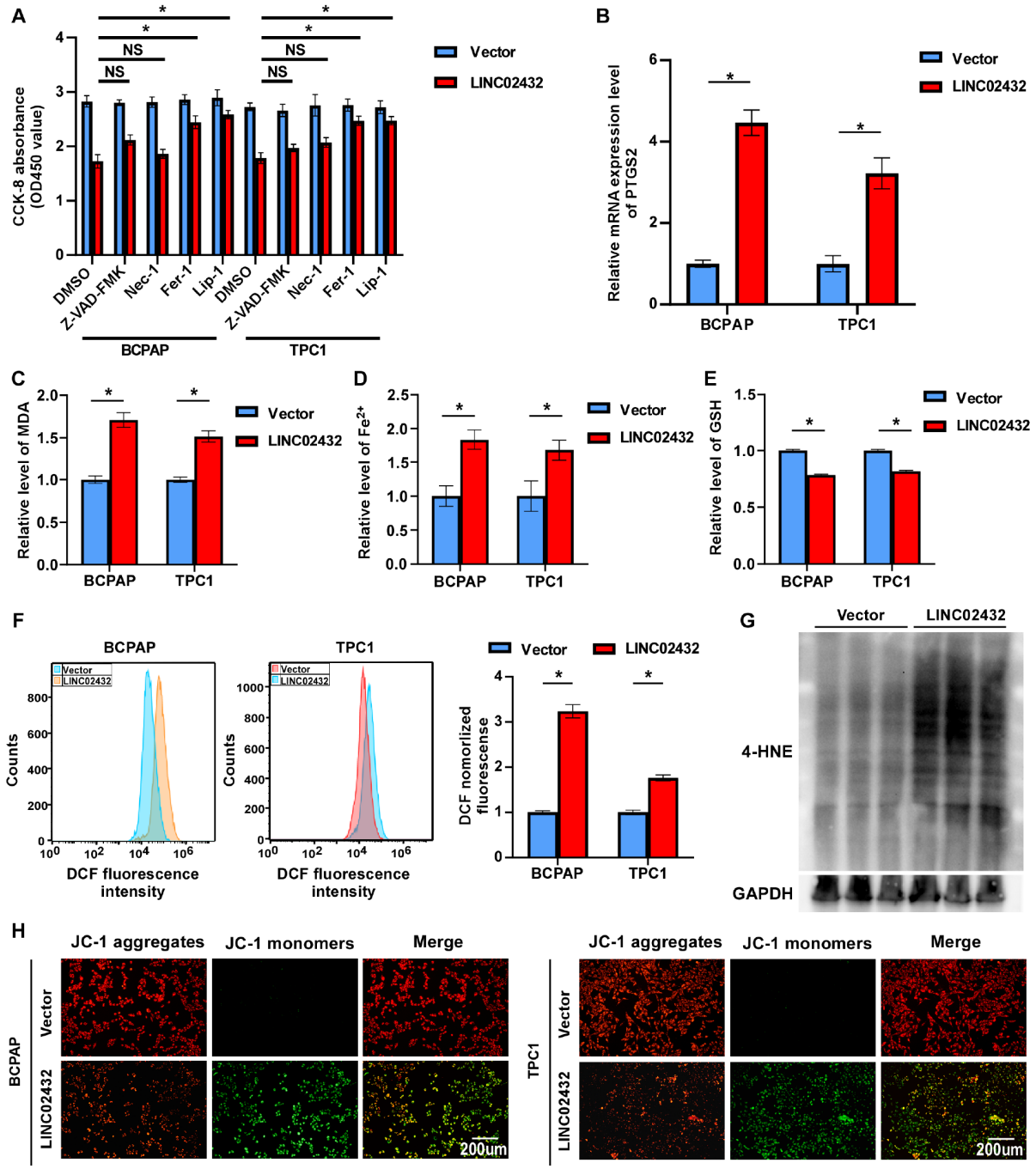


Figure 7. LINC02432 overexpression induces ferroptosis in PTC cells (A) CCK-8 assays were performed on BCPAP and TPC1 cells treated with the apoptosis inhibitor Z-VAD-FMK (10 μM), the necrosis inhibitor Nec-1 (10 μM), the ferroptosis inhibitor Fer-1 (2 μM), or Lip-1 (0.2 μM) for 24 h. (B) qRT-PCR analysis of PTGS2 expression levels. (C) Relative levels of MDA in the indicated cells. (D) Measurement of Fe^{2+} in the indicated cells. (E) Assessment of GSH in the indicated cells. (F) Intracellular ROS production was measured via flow cytometry. (G) Western blot analysis demonstrating the levels of the lipid peroxidation product 4-HNE. (H) The mitochondrial membrane potential (MMP) was evaluated via JC-1 staining and visualized via fluorescence microscopy. Representative images are shown (green, JC-1 monomer; red, JC-1 polymer; scale bar, 200 μm). The data are presented as the mean ± SD from three independent experiments. A P value of ≥ 0.05 was considered not significant (NS); $^*P < 0.05$ indicates statistical significance.

tion of NRF2 by upregulating KEAP1, whereas knockdown of *LINC02432* has the opposite effects.

Discussion

Ferroptosis is a distinct form of regulated cell death characterized by iron-dependent lipid peroxidation, leading to ROS accumulation within cells [5]. Recent studies have demonstrated that ferroptosis-inducing pathways play important roles in suppressing tumorigenesis and enhancing the efficacy of targeted therapies, chemotherapy, and immunotherapy [28,29]. LncRNAs have also emerged as crucial

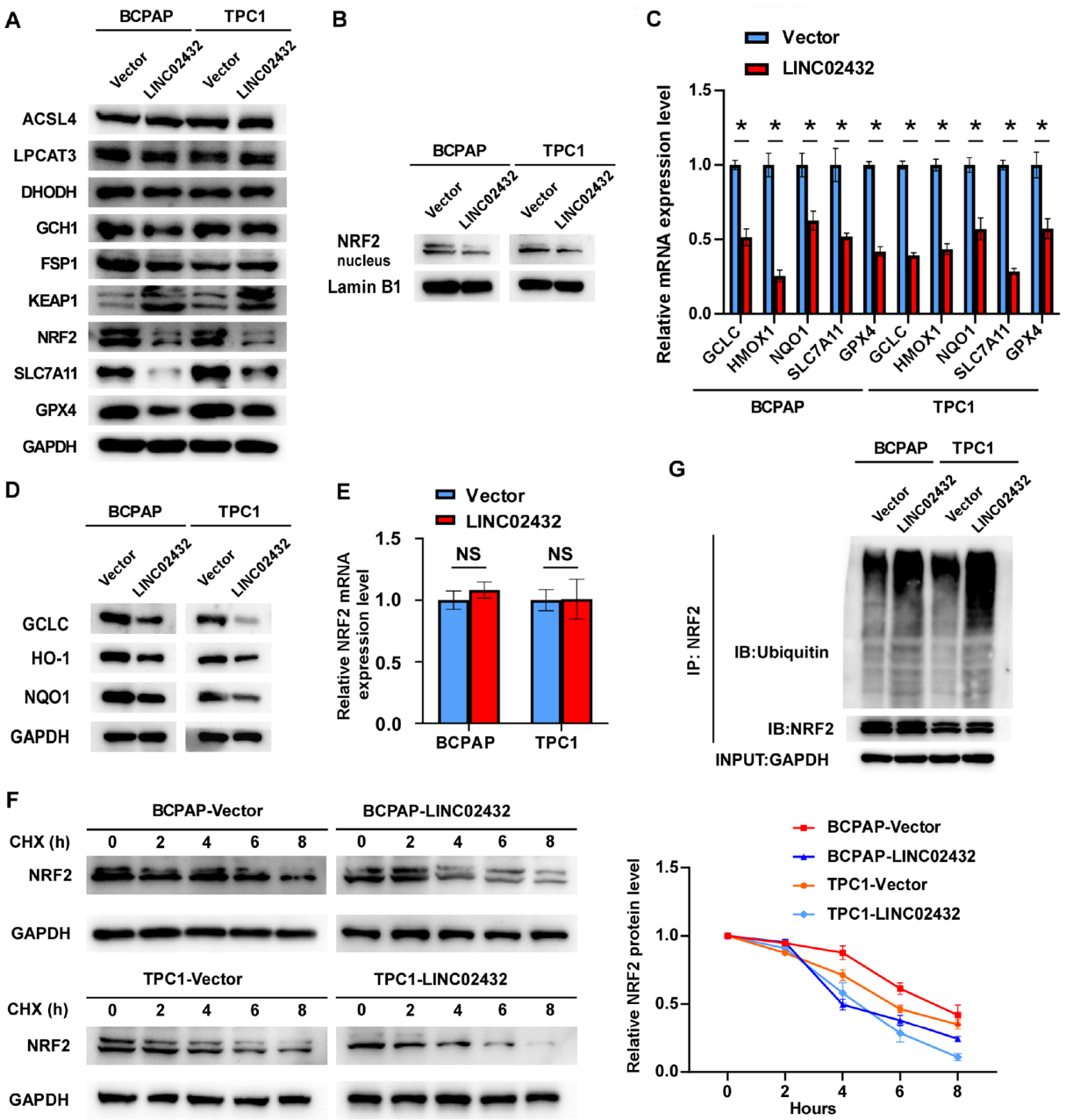


Figure 8. LINC02432 promotes NRF2 ubiquitination and proteasomal degradation in BCPAP and TPC1 cells (A) Western blot analysis of ferroptosis-related proteins. (B) Western blot analysis of NRF2 in the nuclear fractions of the indicated cells. (C) Quantitative reverse transcription PCR (qRT-PCR) analysis of the expression levels of *GCLC*, *HMOX1*, *NQO1*, *SLC7A11*, and *GPX4* in the indicated cells. (D) Western blot analysis showing the protein levels of NRF2 downstream genes (*GCLC*, *HO-1*, *NQO1*) in the indicated cells. (E) qRT-PCR analysis of the *NRF2* mRNA expression levels in the indicated cells. (F) Western blot analysis of NRF2 protein levels in PTC cells treated with 50 μg/mL cycloheximide (CHX) at the indicated time points. (G) Immunoprecipitation analysis of NRF2 ubiquitination levels; all cells were treated with 10 μM MG132 for 6 h. The data are presented as the mean ± SD from three independent experiments. A P value of ≥ 0.05 was considered not significant (NS); *$P < 0.05$ indicates statistical significance.

regulators in cancer biology, influencing gene expression and various biological processes, including ferroptosis [30]. In this study, we analyzed transcriptome data from the TCGA database to identify ferroptosis-related lncRNAs in PTC. After conducting differential expression, survival, and correlation analyses, we identified 66 ferroptosis-related lncRNAs. Remarkably, LINC02432 emerged as the only lncRNA consistently identified across the 10 machine learning methods. These findings emphasize the potential significance of LINC02432 as a critical biomarker in PTC, highlighting the necessity for further study of its clinical and biological roles.

Our data revealed that LINC02432 expression is significantly reduced in PTC tissues and is negatively associated with pathological features. Our analysis of TCGA data, which included 495 PTC samples and 49 adjacent normal tissues, revealed a significant reduction in LINC02432 expression in PTC. The TCGA is a robust resource for cancer research and has a substantial sample size.

Notably, our analysis of 16 paired clinical samples also yielded consistent results, demonstrating a significant reduction in LINC02432 expression in PTC. However, we recognize the limitations of validating these findings with only 16 paired samples, as this may not fully capture the heterogeneity present in PTC. Furthermore, LINC02432 expression is correlated with thyroid cancer differentiation indicators. Interestingly, ferroptosis has been shown to adversely affect differentiation [31]. These observations suggest that LINC02432 is a potential biomarker for PTC.

We conducted a series of experiments to further investigate the role of LINC02432 in PTC. Our results demonstrated that overexpression of LINC02432 inhibited cell proliferation, invasion, and migration. We also found that LINC02432 overexpression was positively associated with ferroptosis. Moreover, knockdown of *LINC02432* had the opposite effects. Given that previous studies have indicated that inhibiting ferroptosis can facilitate tumor growth and metastasis [32], our findings support that LINC02432 exerts its tumor-suppressive effects by promoting ferroptosis in PTC.

At the molecular level, various antioxidant proteins and pathways play crucial roles in regulating ferroptosis, primarily by limiting lipid peroxide production [33]. Inactivation of key regulators such as GPX4 and SLC7A11 leads to glutathione depletion, triggering lipid peroxidation and ferroptosis [33]. As downstream targets of NRF2, GPX4, and SLC7A11 highlight the critical role of NRF2 in modulating the cellular antioxidant response [25]. NRF2, as a master regulator of oxidative stress, activates target genes such as *HMOX1* and *NQO1*, thereby modulating cytoprotective mechanisms [34]. It plays an essential role in counteracting ferroptosis by restoring redox balance through the induction of autophagy and the regulation of iron homeostasis and glutathione metabolism [35,36].

Moreover, ferroptosis suppressor proteins, including FSP1, DHODH, and GCH1, are known for their capacity to reduce oxidative stress by sequestering lipid peroxides [37–39]. On the other hand, LPCAT1 plays a vital role in membrane phospholipid remodeling, which is essential for maintaining cellular redox homeostasis [40]. Our qRT-PCR and western blot analysis results confirmed that LINC02432 promotes ferroptosis by inhibiting the NRF2 pathway via the upregulation of KEAP1, leading to NRF2 ubiquitination and proteasomal degradation.

KEAP1 is regulated within cells through a variety of mechanisms that influence its function and expression [41]. At the transcriptional level, *KEAP1* expression is directly modulated by promoter methylation, particularly within CpG island regions [42]. In addition, microRNAs (miRNAs) represent another layer of regulation. These short, single-stranded noncoding RNAs bind to complementary sequences in the 3′ untranslated region (3′UTR) of target mRNAs, including KEAP1, leading to either mRNA degradation or the suppression of protein translation [43]. In addition to transcriptional and posttranscriptional regulation, KEAP1 expression and activity are also influenced by selective autophagy. p62 facilitates KEAP1 degradation via autophagic processes, allowing the nuclear translocation of NRF2 [44]. Furthermore, KEAP1 is subject to regulation through various posttranslational modifications, such as oxidative alterations, glycosylation, and alkylation, which can affect its stability and functionality [45]. These diverse regulatory mechanisms highlight the intricate control governing KEAP1 activity in response to cellular environmental cues and stress factors. LINC02432's dual localization in both the nuclear and cytoplasmic compartments suggests potentially distinct mechanisms for regulating NRF2 in these different cellular environments. In the cytoplasm, LINC02432 may function as a competitive endogenous RNA (ceRNA) or a "miRNA sponge". By binding to specific microRNAs, LINC02432 is able to alleviate the miRNA-mediated repression of KEAP1, thereby increasing KEAP1 protein level. Moreover, its nuclear localization suggests that LINC02432 may be involved in regulating gene transcription through epigenetic mechanisms. Nuclear lncRNAs are known to associate with chromatin-modifying enzymes, such as DNA methyltransferases (DNMTs), histone-modifying enzymes, and chromatin-remodeling complexes, to influence gene promoter activity [46]. In this context, it is possible that LINC02432 could interact with DNMTs, potentially reducing *KEAP1* promoter methylation, thereby facilitating *KEAP1* transcription. However, the specific mechanism through which LINC02432 regulates KEAP1 remains to be elucidated, indicating a promising avenue for future research.

In conclusion, our study highlights the significant role of LINC02432 as a potential biomarker and therapeutic target in PTC through the promotion of ferroptosis via the inhibition of the NRF2 pathway. The downregulation of LINC02432 in PTC tissues and its association with pathological features further emphasize its tumor-suppressive function. Our findings underline the importance of ferroptosis-related mechanisms in cancer biology and suggest that targeting LINC02432 and its regulatory pathways could offer novel strategies for PTC treatment. Future research should focus on elucidating the detailed mechanisms of the interaction of LINC02432 with KEAP1 and its implications in ferroptosis regulation.

Supplementary Data

Supplementary data are available at *Acta Biochimica et Biophysica Sinica* online.

Funding

This work was supported by the grants from the National Natural Science Foundation of China (No. 82203128) and the Guangdong Basic and Applied Basic Research Fund (Nos. 2023A1515111069 and 2025A1515012538).

Conflict of Interest

The authors declare that they have no conflict of interest.

References

1. Sung H, Ferlay J, Siegel RL, Laversanne M, Soerjomataram I, Jemal A, Bray F. Global cancer statistics 2020: GLOBOCAN estimates of incidence and mortality worldwide for 36 cancers in 185 countries. *CA Cancer J Clin* 2021, 71: 209–249
2. Seib CD, Sosa JA. Evolving understanding of the epidemiology of thyroid cancer. *Endocrinol Metab Clin N Am* 2019, 48: 23–35
3. Guan H, Guo Y, Liu L, Ye R, Liang W, Li H, Xiao H, *et al.* INAVA promotes aggressiveness of papillary thyroid cancer by upregulating MMP9 expression. *Cell Biosci* 2018, 8: 26
4. Lee JJ, Wang TY, Liu CL, Chien MN, Chen MJ, Hsu YC, Leung CH, *et al.* Dipeptidyl peptidase IV as a prognostic marker and therapeutic target in papillary thyroid carcinoma. *J Clin Endocrinol Metab* 2017, 102: 2930–2940
5. Jiang X, Stockwell BR, Conrad M. Ferroptosis: mechanisms, biology and role in disease. *Nat Rev Mol Cell Biol* 2021, 22: 266–282
6. Chen Y, Pan G, Wu F, Zhang Y, Li Y, Luo D. Ferroptosis in thyroid cancer: potential mechanisms, effective therapeutic targets and predictive

biomarker. *Biomed Pharmacother* 2024, 177: 116971
7. Li H, Yang P, Wang JH, Zhang J, Ma Q, Jiang Y, Wu Y, ***et al.*** HLF regulates ferroptosis, development and chemoresistance of triple-negative breast cancer by activating tumor cell-macrophage crosstalk. *J Hematol Oncol* 2022, 15: 2
8. Ross CJ, Ulitsky I. Discovering functional motifs in long noncoding RNAs. *WIREs RNA* 2022, 13: e1708
9. Schmitt AM, Chang HY. Long noncoding RNAs in cancer pathways. *Cancer Cell* 2016, 29: 452–463
10. Saeedi Borujeni MJ, Esfandiary E, Baradaran A, Valiani A, Ghanadian M, Codoñer-Franch P, Basirat R, ***et al.*** Molecular aspects of pancreatic β-cell dysfunction: oxidative stress, microRNA, and long noncoding RNA. *J Cell Physiol* 2019, 234: 8411–8425
11. Yarani R, Mirza AH, Kaur S, Pociot F. The emerging role of lncRNAs in inflammatory bowel disease. *Exp Mol Med* 2018, 50: 1–14
12. Choy M, Guo Y, Li H, Wei G, Ye R, Liang W, Xiao H, ***et al.*** Long noncoding RNA LOC100129940-N is upregulated in papillary thyroid cancer and promotes the invasion and progression. *Int J Endocrinol* 2019, 2019: 1–12
13. Rombaut D, Chiu HS, Decaesteker B, Everaert C, Yigit N, Peltier A, Janoueix-Lerosey I, ***et al.*** Integrative analysis identifies lincRNAs up- and downstream of neuroblastoma driver genes. *Sci Rep* 2019, 9: 5685
14. Wang X, Cheng H, Zhao J, Li J, Chen Y, Cui K, Tian L, ***et al.*** Long noncoding RNA DLGAP1-AS2 promotes tumorigenesis and metastasis by regulating the Trim21/ELOA/LHPP axis in colorectal cancer. *Mol Cancer* 2022, 21: 210
15. Murugan AK, Munirajan AK, Alzahrani AS. Long noncoding RNAs: emerging players in thyroid cancer pathogenesis. *Endocrine-Relat Cancer* 2018, 25: R59–R82
16. Cho SW, Xu J, Sun R, Mumbach MR, Carter AC, Chen YG, Yost KE, ***et al.*** Promoter of lncRNA gene PVT1 is a tumor-suppressor DNA boundary element. *Cell* 2018, 173: 1398–1412.e22
17. Zhou N, Bao J. FerrDb: a manually curated resource for regulators and markers of ferroptosis and ferroptosis-disease associations. *Database* 2020, 2020: baaa021
18. Tuttle RM, Ahuja S, Avram AM, Bernet VJ, Bourguet P, Daniels GH, Dillehay G, ***et al.*** Controversies, consensus, and collaboration in the use of ^{131}I therapy in differentiated thyroid cancer: a joint statement from the american thyroid association, the european association of nuclear medicine, the society of nuclear medicine and molecular imaging, and the european thyroid association. *Thyroid* 2019, 29: 461–470
19. Kang N, Zhao Z, Wang Z, Ning J, Wang H, Zhang W, Ruan X, ***et al.*** METTL3 regulates thyroid cancer differentiation and chemosensitivity by modulating PAX8. *Int J Biol Sci* 2024, 20: 3426–3441
20. Pu W, Shi X, Yu P, Zhang M, Liu Z, Tan L, Han P, ***et al.*** Single-cell transcriptomic analysis of the tumor ecosystems underlying initiation and progression of papillary thyroid carcinoma. *Nat Commun* 2021, 12: 6058
21. Wang L, Park HJ, Dasari S, Wang S, Kocher JP, Li W. CPAT: coding-potential assessment tool using an alignment-free logistic regression model. *Nucleic Acids Res* 2013, 41: e74
22. Kong L, Zhang Y, Ye ZQ, Liu XQ, Zhao SQ, Wei L, Gao G. CPC: assess the protein-coding potential of transcripts using sequence features and support vector machine. *Nucleic Acids Res* 2007, 35: W345–W349
23. Wei C, Xu Y, Shen Q, Li R, Xiao X, Saw PE, Xu X. Role of long non-coding RNAs in cancer: from subcellular localization to nanoparticle-mediated targeted regulation. *Mol Ther Nucleic Acids* 2023, 33: 774–793
24. Zhou Q, Meng Y, Li D, Yao L, Le J, Liu Y, Sun Y, ***et al.*** Ferroptosis in cancer: from molecular mechanisms to therapeutic strategies. *Sig Transduct Target Ther* 2024, 9: 55
25. Schmidlin CJ, Shakya A, Dodson M, Chapman E, Zhang DD. The intricacies of NRF2 regulation in cancer. *Semin Cancer Biol* 2021, 76: 110–119
26. Yamamoto M, Kensler TW, Motohashi H. The KEAP1-NRF2 system: a thiol-based sensor-effector apparatus for maintaining redox homeostasis. *Physiol Rev* 2018, 98: 1169–1203
27. Zhang DD, Lo SC, Cross JV, Templeton DJ, Hannink M. Keap1 is a redox-regulated substrate adaptor protein for a Cul3-dependent ubiquitin ligase complex. *Mol Cell Biol* 2004, 24: 10941–10953
28. Chen F, Kang R, Tang D, Liu J. Ferroptosis: principles and significance in health and disease. *J Hematol Oncol* 2024, 17: 41
29. Liu B, Chen Z, Li Z, Zhao X, Zhang W, Zhang A, Wen L, ***et al.*** Hsp90α promotes chemoresistance in pancreatic cancer by regulating Keap1-Nrf2 axis and inhibiting ferroptosis. *Acta Biochim Biophys Sin* 2024, 57: 295–309
30. Nejadi Orang F, Abdoli Shadbad M. Competing endogenous RNA networks and ferroptosis in cancer: novel therapeutic targets. *Cell Death Dis* 2024, 15: 357
31. Luo C, Xu W, Tang X, Liu X, Cheng Y, Wu Y, Xie Z, ***et al.*** Canonical Wnt signaling works downstream of iron overload to prevent ferroptosis from damaging osteoblast differentiation. *Free Radical Biol Med* 2022, 188: 337–350
32. Zheng X, Chen W, Yi J, Li W, Liu J, Fu W, Ren L, ***et al.*** Apolipoprotein C1 promotes glioblastoma tumorigenesis by reducing KEAP1/NRF2 and CBS-regulated ferroptosis. *Acta Pharmacol Sin* 2022, 43: 2977–2992
33. Dixon SJ, Olzmann JA. The cell biology of ferroptosis. *Nat Rev Mol Cell Biol* 2024, 25: 424–442
34. Krajka-Kuźniak V, Paluszczak J, Baer-Dubowska W. The Nrf2-ARE signaling pathway: an update on its regulation and possible role in cancer prevention and treatment. *Pharmacol Rep* 2017, 69: 393–402
35. Tang D, Chen X, Kang R, Kroemer G. Ferroptosis: molecular mechanisms and health implications. *Cell Res* 2021, 31: 107–125
36. Sajadimajd S, Khazaei M. Oxidative stress and cancer: the role of Nrf2. *Curr Cancer Drug Targets* 2018, 18: 538–557
37. Mao C, Liu X, Zhang Y, Lei G, Yan Y, Lee H, Koppula P, ***et al.*** DHODH-mediated ferroptosis defence is a targetable vulnerability in cancer. *Nature* 2021, 593: 586–590
38. Tang Z, Liu L, Guo Y, Deng G, Chen M, Wei J. Exendin-4 reverses endothelial dysfunction in mice fed a high-cholesterol diet by a GTP cyclohydrolase-1/tetrahydrobiopterin pathway. *Mol Med Report* 2018
39. Doll S, Freitas FP, Shah R, Aldrovandi M, da Silva MC, Ingold I, Goya Grocin A, ***et al.*** FSP1 is a glutathione-independent ferroptosis suppressor. *Nature* 2019, 575: 693–698
40. Li Z, Hu Y, Zheng H, Li M, Liu Y, Feng R, Li X, ***et al.*** LPCAT1-mediated membrane phospholipid remodelling promotes ferroptosis evasion and tumour growth. *Nat Cell Biol* 2024, 26: 811–824
41. Chen F, Xiao M, Hu S, Wang M. Keap1-Nrf2 pathway: a key mechanism in the occurrence and development of cancer. *Front Oncol* 2024, 14: 1381467
42. Fabrizio FP, Mazza T, Castellana S, Sparaneo A, Muscarella LA. Epigenetic scanning of *KEAP1* CpG sites uncovers new molecular-driven patterns in lung adeno and squamous cell carcinomas. *Antioxidants* 2020, 9: 904
43. Shen K, Wang X, Wang Y, Jia Y, Zhang Y, Wang K, Luo L, ***et al.*** miR-125b-5p in adipose derived stem cells exosome alleviates pulmonary microvascular endothelial cells ferroptosis via Keap1/Nrf2/GPX4 in sepsis lung injury. *Redox Biol* 2023, 62: 102655
44. Zhang W, Geng X, Dong Q, Li X, Ye P, Lin M, Xu B, ***et al.*** Crosstalk between autophagy and the Keap1-Nrf2-ARE pathway regulates realgar-induced neurotoxicity. *J EthnoPharmacol* 2023, 301: 115776
45. Ohnuma T, Nakayama S, Anan E, Nishiyama T, Ogura K, Hiratsuka A. Activation of the Nrf2/ARE pathway via S-alkylation of cysteine 151 in the chemopreventive agent-sensor Keap1 protein by falcarindiol, a conjugated diacetylene compound. *Toxicol Appl Pharmacol* 2010, 244: 27–36
46. Wang X, Zenda T, Liu S, Liu G, Jin H, Dai L, Dong A, ***et al.*** Comparative proteomics and physiological analyses reveal important maize filling-kernel drought-responsive genes and metabolic pathways. *Int J Mol Sci* 2019, 20: 3743